Eur. Phys. J. C 50, 29–34 (2007)
DOI 10.1140/epjc/s10052-006-0189-z

THE EUROPEAN PHYSICAL JOURNAL C

Regular Article – Theoretical Physics

The curvature of $F_2^p(x,Q^2)$ as a probe of the range of validity of perturbative QCD evolutions in the small-x region

M. Glück[1], C. Pisano[2,a], E. Reya[1]

[1] Universität Dortmund, Institut für Physik, 44221 Dortmund, Germany
[2] Universität Hamburg, II. Institut für Theoretische Physik, Luruper Chaussee 149, 22761 Hamburg, Germany

Received: 5 October 2006 / Revised version: 17 November 2006 /
Published online: 24 January 2007 –

Abstract. Perturbative NLO and NNLO QCD evolutions of parton distributions are studied, in particular in the (very) small-x region, where they are in very good agreement with all recent precision measurements of $F_2^p(x,Q^2)$. These predictions turn out to be also rather insensitive to the specific choice of the factorization scheme ($\overline{\rm MS}$ or DIS). A characteristic feature of perturbative QCD evolutions is a *positive* curvature of F_2^p which increases as x decreases. This perturbatively stable prediction provides a sensitive test of the range of validity of perturbative QCD.

1 Introduction

The curvature of DIS structure functions like $F_2^p(x,Q^2)$, i.e., its second derivative with respect to the photon's virtuality Q^2 at fixed values of x, plays a decisive role in probing the range of validity of perturbative QCD evolutions of parton distributions in the small-x region. This has been observed recently [1, 2] and it was demonstrated that NLO($\overline{\rm MS}$) evolutions imply a *positive* curvature which increases as x decreases. However, in contrast to [1] where this positive curvature was shown to disagree with the data, the conventional *full* NLO analysis performed in [2] led to the conclusion that no such disagreement prevails. It was therefore concluded [2] that the NLO small-x parton evolution equations are *not* challenged by the small-x data on F_2^p. These rather unique predictions provide a check of the range of validity of perturbative QCD evolutions. However, the curvature is a rather subtle mathematical quantity which a priori may sensitively depend on the theoretical (non-) perturbative assumptions made for calculating it. The main purpose of the present article is to study the dependence and stability of the predicted curvature with respect to a different choice of the factorization scheme (DIS versus $\overline{\rm MS}$) and to the perturbative order of the evolutions by extending the common NLO (2-loop) evolution [2] to the next-to-next-to-leading 3-loop order (NNLO).

2 Theoretical formalism

In the common $\overline{\rm MS}$ factorization scheme the relevant F_2^p structure function as extracted from the DIS ep process can be, up to NNLO, written as [3–5]

$$F_2^p(x,Q^2) = F_{2,\rm NS}^+(x,Q^2) + F_{2,\rm S}(x,Q^2) + F_2^c(x,Q^2,m_c^2)\,, \tag{1}$$

with the non-singlet contribution for three active (light) flavors being given by

$$\frac{1}{x}F_{2,\rm NS}^+(x,Q^2) = \left[C_{2,q}^{(0)} + aC_{2,\rm NS}^{(1)} + a^2C_{2,\rm NS}^{(2)+}\right] \otimes \left[\frac{1}{18}q_8^+ + \frac{1}{6}q_3^+\right](x,Q^2)\,, \tag{2}$$

where $a = a(Q^2) \equiv \alpha_{\rm s}(Q^2)/4\pi$, $C_{2,q}^{(0)}(z) = \delta(1-z)$, $C_{2,\rm NS}^{(1)}$ is the common NLO coefficient function (see, for example, [6]) and a convenient expression for the relevant NNLO 2-loop Wilson coefficient $C_{2,\rm NS}^{(2)+}$ can be found in [3]. The NNLO Q^2-evolution of the flavor non-singlet combinations $q_3^+ = u+\bar u-(d+\bar d) = u_{\rm v}-d_{\rm v}$ and $q_8^+ = u+\bar u+d+\bar d-2(s+\bar s) = u_{\rm v}+d_{\rm v}+4\bar q-4\bar s$, where $\bar q \equiv \bar u = \bar d$ and $s = \bar s$, is related to the 3-loop splitting function [7] $P_{\rm NS}^{(2)+}$, besides the usual LO (1-loop) and NLO (2-loop) ones, $P_{\rm NS}^{(0)}$ and $P_{\rm NS}^{(1)+}$, respectively [3, 8]. Notice that we do not consider sea breaking effects ($\bar u \neq \bar d$, $s \neq \bar s$), since the HERA data used, and thus our analysis, are not sensitive to such corrections. The flavor singlet contribution in (1) reads

$$\frac{1}{x}F_{2,\rm S}(x,Q^2) = \frac{2}{9}\Big\{\left[C_{2,q}^{(0)} + aC_{2,q}^{(1)} + a^2C_{2,q}^{(2)}\right] \otimes \Sigma + \left[aC_{2,g}^{(1)} + a^2C_{2,g}^{(2)}\right] \otimes g\Big\}(x,Q^2)\,, \tag{3}$$

with $\Sigma(x,Q^2) \equiv \Sigma_{q=u,d,s}(q+\bar q) = u_{\rm v}+d_{\rm v}+4\bar q+2\bar s$, $C_{2,q}^{(1)} = C_{2,\rm NS}^{(1)}$ and the additional common NLO gluonic coefficient

[a] e-mail: pisano@mail.desy.de

function $C_{2,g}^{(1)}$ can be again found in [6], for example. Convenient expressions for the NNLO $C_{2,q}^{(2)}$ and $C_{2,g}^{(2)}$ have been given in [4] and the relevant 3-loop splitting functions $P_{ij}^{(2)}$, required for the evolution of $\Sigma(x,Q^2)$ and $g(x,Q^2)$, have been derived in [9]. We have performed all Q^2-evolutions in Mellin n-moment space and used the QCD-PEGASUS program [10] for the NNLO evolutions. In NNLO the strong coupling evolves according to $\mathrm{d}a/\mathrm{d}\ln Q^2 = -\Sigma_{\ell=0}^{2}\beta_\ell a^{\ell+2}$ where $\beta_0 = 11-2f/3$, $\beta_1 = 102-38f/3$ and $\beta_2 = 2857/2 - 5033f/18 + 325f^2/54$, and the running $a(Q^2)$ is appropriately matched at $Q = m_c = 1.4\,\mathrm{GeV}$ and $Q = m_b = 4.5\,\mathrm{GeV}$. The heavy flavor (charm) contribution F_2^c in (1) is taken as in [2] as given by the fixed-order NLO perturbation theory [11, 12]. The small bottom contribution turns out to be negligible for our purposes. Notice that a NNLO calculation of heavy quark production is not yet available. For definiteness we work in the fixed flavor factorization scheme, given in (1)–(3), rather than in the variable (massless quark) scheme since the results for F_2^p and its curvature remain essentially unchanged [2].

The choice of a factorization scheme in NLO, other than the $\overline{\mathrm{MS}}$ scheme used thus far, might imply similar effects as the additional NNLO contributions in the $\overline{\mathrm{MS}}$ scheme. For example, in the deep inelastic scattering (DIS) factorization scheme [5, 6, 13, 14] the Wilson coefficients in (2) and (3) are absorbed into the parton distributions, or more precisely into their evolutions, i.e., into the splitting functions. Disregarding for simplicity all NNLO contributions, this transformation to the DIS scheme in NLO is achieved via [4, 5]

$$P_{\mathrm{NS}}^{(1)} \to P_{\mathrm{NS,DIS}}^{(1)} = P_{\mathrm{NS}}^{(1)} + \beta_0 \Delta C_{2,\mathrm{NS}}^{(1)}\,, \tag{4}$$

$$\begin{aligned}\widehat{P}^{(1)} \to \widehat{P}_{\mathrm{DIS}}^{(1)} &= \widehat{P}^{(1)} + \beta_0 \Delta\widehat{C}_2^{(1)} \\ &\quad - \left[\Delta\widehat{C}_2^{(1)} \otimes \widehat{P}^{(0)} - \widehat{P}^{(0)} \otimes \Delta\widehat{C}_2^{(1)}\right],\end{aligned} \tag{5}$$

where

$$\Delta C_{2,\mathrm{NS}}^{(1)} = -C_{2,\mathrm{NS}}^{(1)}\,, \quad \Delta\widehat{C}_2^{(1)} = -\begin{pmatrix} C_{2,q}^{(1)} & C_{2,g}^{(1)} \\ -C_{2,q}^{(1)} & -C_{2,g}^{(1)} \end{pmatrix}. \tag{6}$$

Instead of (2) and (3), the light u, d, s quark contributions to F_2^p in the NLO(DIS) factorization scheme now simply become

$$\begin{aligned}F_2^p(x,Q^2) &= x\sum_{q=u,d,s} e_q^2\left[q(x,Q^2)+\bar{q}(x,Q^2)\right]_{\mathrm{DIS}} + F_2^c \\ &= x\left[\frac{1}{18}q_8^+(x,Q^2) + \frac{1}{6}q_3^+(x,Q^2)\right]_{\mathrm{DIS}} \\ &\quad + \frac{2}{9}x\Sigma(x,Q^2)_{\mathrm{DIS}} + F_2^c\,.\end{aligned} \tag{7}$$

The quantitative difference between the NLO($\overline{\mathrm{MS}}$) and NLO(DIS) results will turn out to be rather small. Therefore we do not consider any further the DIS scheme in NNLO.

Having obtained the parton distributions ${}^{(-)}_{q}(x,Q^2)_{\mathrm{DIS}}$ and $g(x,Q^2)_{\mathrm{DIS}}$ from an explicit NLO analysis of $F_2(x,Q^2)$ in the DIS factorization scheme, one can transform them to the $\overline{\mathrm{MS}}$ scheme via (see [15], for example)

$$\begin{aligned}{}^{(-)}_{q}(x,Q^2) &= {}^{(-)}_{q}(x,Q^2)_{\mathrm{DIS}} \\ &\quad - a\left[C_{2,q}^{(1)} \otimes {}^{(-)}_{q}{}_{\mathrm{DIS}} + \frac{1}{2f}C_{2,g}^{(1)} \otimes g_{\mathrm{DIS}}\right](x,Q^2) \\ &\quad + \mathcal{O}(a^2)\,,\end{aligned} \tag{8}$$

$$\begin{aligned}g(x,Q^2) &= g(x,Q^2)_{\mathrm{DIS}} \\ &\quad + a\left[C_{2,q}^{(1)} \otimes \Sigma_{\mathrm{DIS}} + C_{2,g}^{(1)} \otimes g_{\mathrm{DIS}}\right](x,Q^2) \\ &\quad + \mathcal{O}(a^2)\,,\end{aligned} \tag{9}$$

where

$$C_{2,q}^{(1)}(z) = 2\frac{4}{3}\left[\frac{1+z^2}{1-z}\left(\ln\frac{1-z}{z} - \frac{3}{4}\right) + \frac{1}{4}(9+5z)\right]_+\,, \tag{10}$$

$$C_{2,g}^{(1)}(z) = 4f\frac{1}{2}\left[(z^2+(1-z)^2)\ln\frac{1-z}{z} - 1 + 8z(1-z)\right], \tag{11}$$

with $f = 3$. This transformation to the $\overline{\mathrm{MS}}$ scheme then allows for a consistent comparison of our NLO(DIS) results with the higher-order results obtained in the $\overline{\mathrm{MS}}$ factorization scheme.

3 Quantitative results

For the present analysis the valence ($q_{\mathrm{v}} = u_{\mathrm{v}}$, d_{v}) and sea ($w = \bar{q}$, g) distributions are parametrized at an input scale $Q_0^2 = 1.5\,\mathrm{GeV}^2$ as follows:

$$\begin{aligned}xq_{\mathrm{v}}\big(x,Q_0^2\big) &= N_{q_{\mathrm{v}}}x^{a_{q_{\mathrm{v}}}}(1-x)^{b_{q_{\mathrm{v}}}} \\ &\quad \times\left(1 + c_{q_{\mathrm{v}}}\sqrt{x} + d_{q_{\mathrm{v}}}x + e_{q_{\mathrm{v}}}x^{1.5}\right),\end{aligned} \tag{12}$$

$$xw\big(x,Q_0^2\big) = N_w x^{a_w}(1-x)^{b_w}\left(1 + c_w\sqrt{x} + d_w x\right) \tag{13}$$

and without loss of generality the strange sea is taken to be $s = \bar{s} = 0.5\bar{q}$. The normalizations $N_{u_{\mathrm{v}}}$ and $N_{d_{\mathrm{v}}}$ are fixed by $\int_0^1 u_{\mathrm{v}}\,\mathrm{d}x = 2$ and $\int_0^1 d_{\mathrm{v}}\,\mathrm{d}x = 1$, respectively, and N_g is fixed via $\int_0^1 x(\Sigma+g)\,\mathrm{d}x = 1$. We have somewhat extended the set of DIS data used in [2] in order to determine the remaining parameters at larger values of x and of the valence distributions. The following data sets have been used: the small-x [16] and large-x [17] H1 F_2^p data; the fixed target BCDMS data [18, 19] for F_2^p and F_2^n using $Q^2 \geq 20\,\mathrm{GeV}^2$ and $W^2 = Q^2\left(\frac{1}{x}-1\right) + m_p^2 \geq 10\,\mathrm{GeV}^2$ cuts, and the proton and deuteron NMC data [20, 21] for $Q^2 \geq 4\,\mathrm{GeV}^2$ and $W^2 \geq 10\,\mathrm{GeV}^2$. This amounts to a total of 740 data points. The required overall normalization factor of the data turned out to be 0.98 for BCDMS and 1.0 for NMC. The resulting parameters of the various fits are summarized in Table 1. The relevant small-x predictions are compared with the H1 data [16] in Fig. 1, which are also consistent with the ZEUS data [22] with partly lower

Table 1. Parameter values of the NLO and NNLO QCD fits with the parameters of the input distributions referring to (12) and (13). Here χ^2 was evaluated by adding in quadrature the statistical and systematic errors

	NNLO($\overline{\rm MS}$)				NLO($\overline{\rm MS}$)				NLO(DIS)			
	$u_{\rm v}$	$d_{\rm v}$	$\bar{q}$	g	$u_{\rm v}$	$d_{\rm v}$	$\bar{q}$	g	$u_{\rm v}$	$d_{\rm v}$	$\bar{q}$	g
N	0.2503	3.6204	0.1196	2.1961	0.4302	0.3959	0.0546	2.3780	0.6885	0.4476	0.0702	2.3445
a	0.2518	0.9249	−0.1490	−0.0121	0.2859	0.5375	−0.2178	−0.0121	0.3319	0.5215	−0.1960	−0.0121
b	3.6287	6.7111	3.7281	6.5144	3.5503	5.7967	3.3107	5.6392	2.6511	2.290	5.5480	6.8581
c	4.7636	6.7231	0.6210	2.0917	1.1120	22.495	5.3095	0.8792	−1.6163	10.398	3.7277	1.8732
d	24.180	−24.238	−1.1350	−3.0894	15.611	−52.702	−5.9049	−1.7714	15.197	−16.466	−4.7067	−2.4302
e	9.0492	30.106	–	–	4.2409	69.763	–	–	−7.6056	5.6364	–	–
χ^2/dof	0.989				0.993				0.992			
$\alpha_{\rm s}(M_Z^2)$	0.112				0.114				0.114			

statistics. The present more detailed NLO($\overline{\rm MS}$) analysis corresponds to $\chi^2/{\rm dof} = 715.3/720$ and the results are comparable to our previous ones [2]. Our new NLO(DIS) and NNLO(3-loop) fits are also very similar, corresponding to $\chi^2/{\rm dof} = 714.2/720$ and $712.0/720$, respectively, although they fall slightly below the common NLO($\overline{\rm MS}$) predictions at smaller values of Q^2. It should be emphasized that the perturbatively stable QCD predictions are in perfect agreement with all recent high-statistics measurements of the Q^2-dependence of $F_2^p(x,Q^2)$ in the (very) small-x region. Therefore additional model assumptions concerning further resummations of subleading small-x logarithms (see, for example, [23]) are not required [7, 9].

In Figs. 2 and 3 we show our gluon and sea input distributions in (13) and Table 1 as obtained in our three different fits, as well as their evolved shapes at $Q^2 = 4.5\ {\rm GeV}^2$ in particular in the small-x region. In order to allow for a consistent comparison in the $\overline{\rm MS}$ scheme, our NLO(DIS) results have been transformed to the $\overline{\rm MS}$ factorization scheme using (8) and (9). Note, however, that the gluon distribution in the DIS scheme is very similar to the one obtained in NLO($\overline{\rm MS}$) shown in Fig. 2 which holds in particular in the small-x region. This agreement becomes even

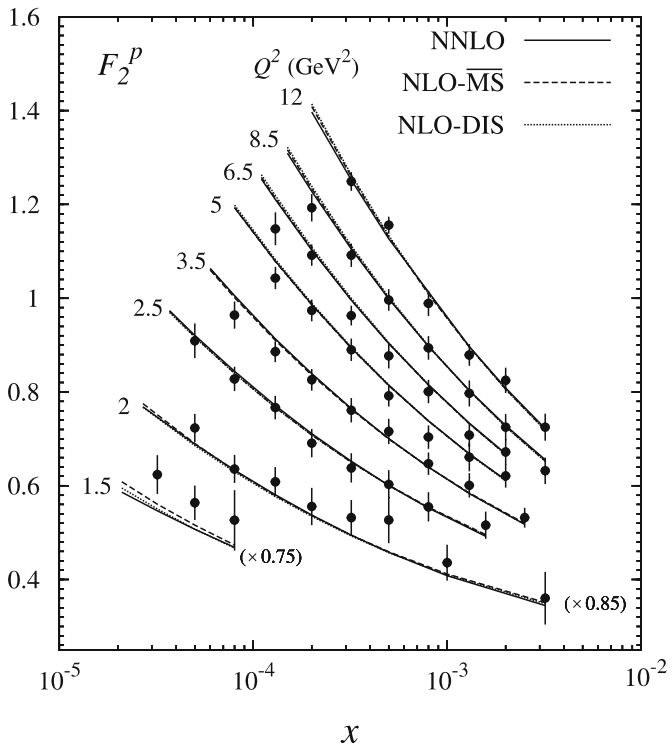

Fig. 1. Comparison of our various perturbative fits with the H1 data [16] at very small-x. Our 3-loop NNLO results always refer to the $\overline{\rm MS}$ factorization scheme. To ease the graphical representation, the results and data for the lowest two bins in Q^2 have been multiplied by the numbers as indicated

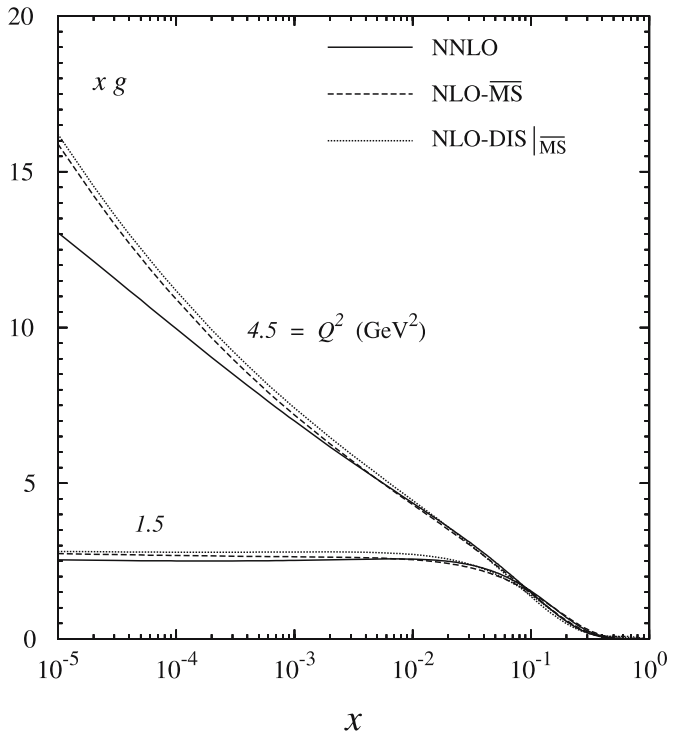

Fig. 2. The gluon distributions at the input scale $Q_0^2 = 1.5\,{\rm GeV}^2$, corresponding to (13) with the parameters given in Table 1, and at $Q^2 = 4.5\,{\rm GeV}^2$. For a consistent comparison with the NNLO and NLO results in the $\overline{\rm MS}$ factorization scheme, we have transformed our NLO-DIS results to the $\overline{\rm MS}$ scheme using (9) which are denoted by NLO-DIS$|_{\overline{\rm MS}}$

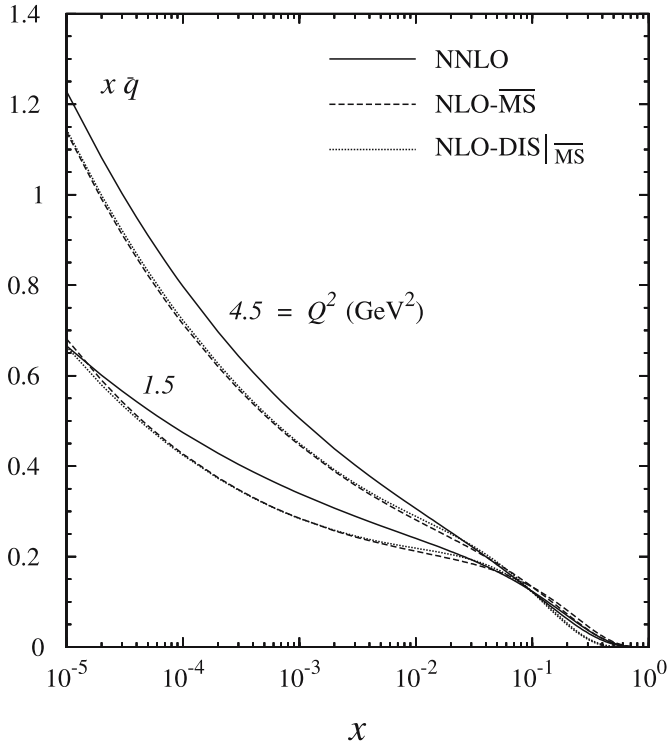

Fig. 3. As in Fig. 2, but for the sea distribution $x\bar{q}(x,Q^2)$ where $\bar{q} \equiv \bar{u} = \bar{d}$. The NLO-DIS results have been transformed to the $\overline{\rm MS}$ factorization scheme using (8); they are denoted by NLO-DIS$|_{\overline{\rm MS}}$

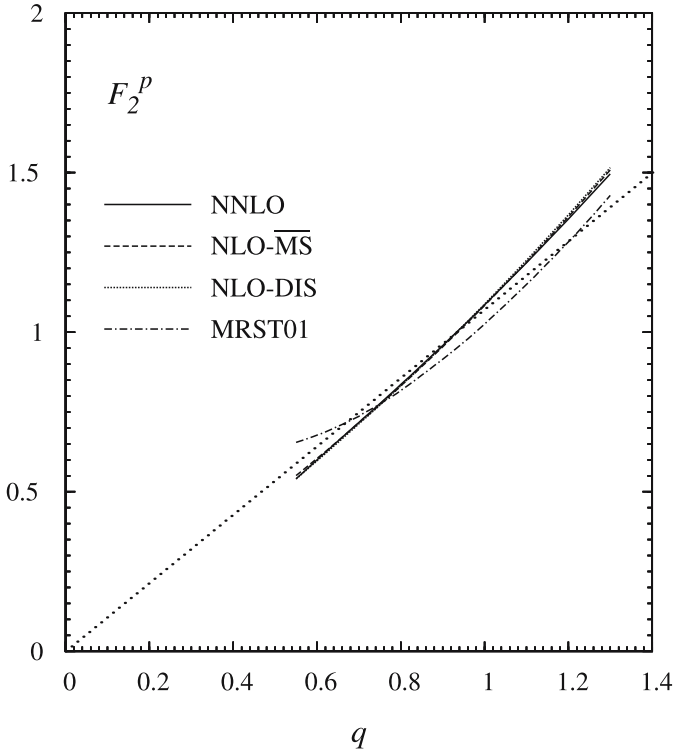

Fig. 4. Predictions for $F_2^p(x,Q^2)$ at $x = 10^{-4}$ plotted versus q defined in (14). For comparison the global fit NLO result of MRST01 [24] is shown as well. The global CTEQ6M NLO fit [25] is very similar to our NLO and NNLO results as can be deduced from [2], and the same holds true for the H1 fit [17]. Most small-x data lie along the *straight dotted line* [1]

better for increasing values of Q^2. This agreement is similar for the sea distributions in the small-x region shown in Fig. 3. Only for $x \gtrsim 0.1$ the NLO(DIS) sea density becomes sizeably smaller than the NLO($\overline{\rm MS}$) one shown in Fig. 3. The NLO results are rather similar but distinctively different from the NNLO ones in the very small-x region at $Q^2 > Q_0^2$. In particular the strong increase of the gluon distribution $xg(x,Q^2)$ as $x \to 0$ at NLO is somewhat tamed by NNLO 3-loop effects [9].

Turning now to the curvature of F_2^p we first present in Fig. 4 our results for $F_2^p(x,Q^2)$ at $x = 10^{-4}$, together with a global fit MRST01 NLO result [24], as a function of [1]

$$q = \log_{10}\left(1 + \frac{Q^2}{0.5\ \mathrm{GeV}^2}\right). \qquad (14)$$

This variable has the advantage that most measurements lie along a straight line [1] as indicated by the dotted line in Fig. 4. All our three NLO and NNLO fits give almost the same results which are also very similar [2] to the global CTEQ6M NLO fit [25]. In contrast to all other fits shown in Fig. 4, only the MRST01 parametrization results in a sizeable curvature for F_2^p [2]. More explicitly the curvature can be directly extracted from

$$F_2^p(x,Q^2) = a_0(x) + a_1(x)q + a_2(x)q^2. \qquad (15)$$

The curvature $a_2(x) = \frac{1}{2}\partial_q^2 F_2^p(x,Q^2)$ is evaluated by fitting this expression to the predictions for $F_2^p(x,Q^2)$ at fixed values of x to a (kinematically) given interval of q. In Fig. 5a we present $a_2(x)$ which results from experimentally selected q-intervals [1, 2]:

$$\begin{aligned} &0.7 \le q \le 1.4 \quad &&\text{for} \quad 2\times10^{-4} < x < 10^{-2}, \\ &0.7 \le q \le 1.2 \quad &&\text{for} \quad 5\times10^{-5} < x \le 2\times10^{-4}. \end{aligned} \qquad (16)$$

It should be noticed that the average value of q decreases with decreasing x due to the kinematically more restricted Q^2 range accessible experimentally. (We deliberately do not show the results at the smallest available $x = 5\times10^{-5}$ where the q-interval is too small, $0.6 \le q \le 0.8$, for fixing $a_2(x)$ in (15) uniquely and where moreover present measurements are not yet sufficiently accurate [1, 2].) For comparison we also show in Fig. 5b the curvature $a_2(x)$ for an x-independent fixed q-interval

$$0.6 \le q \le 1.4 \quad (1.5 \le Q^2 \le 12\ \mathrm{GeV}^2). \qquad (17)$$

Apart from the rather large values of $a_2(x)$ specific [2] for the MRST01 fit, our NLO and NNLO results agree well with the experimental curvatures as calculated and presented in [1] using the H1 data [16]. Our predictions do *not* sensitively depend on the factorization scheme chosen ($\overline{\rm MS}$ or DIS) and are, moreover, perturbative *stable* with the NNLO 3-loop results lying typically below the NLO ones, i.e. closer to present data. It should be emphasized that the perturbative stable evolutions always result in a *posi-*

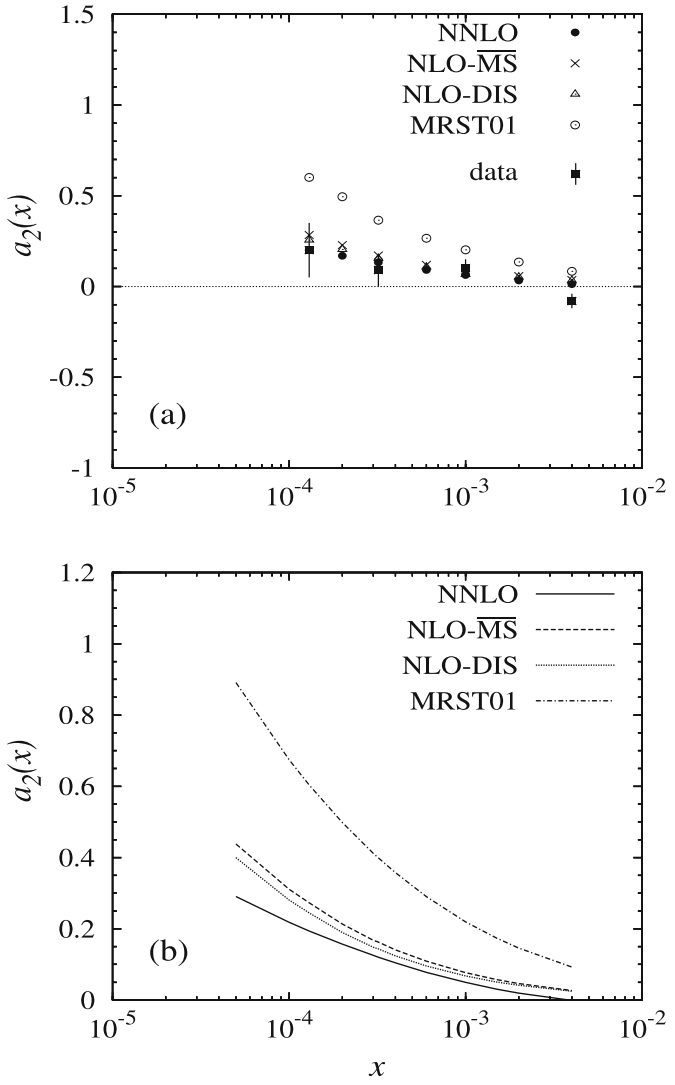

Fig. 5. The curvature $a_2(x)$ as defined in (15) for **a** the variable q-intervals in (16) and **b** the fixed q-interval in (17). Also shown are the corresponding MRST01 NLO results [24]. The data in **a** are taken from [1]. The NNLO prediction at the lowest x-value coincides with the data (*full square*)

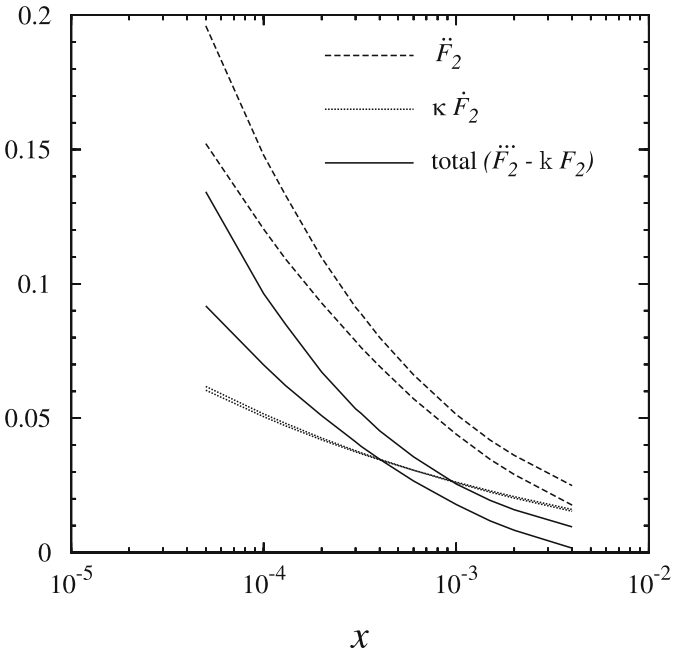

Fig. 6. The predicted slope $\dot{F}_2^p \equiv \partial F_2^p/\partial \ln Q^2$ and curvature $\ddot{F}_2^p$ appearing in (18) for the fixed q-interval in (17), with the suppression factor $\kappa = 0.1$ corresponding to an average $Q^2 = 4.5\,\mathrm{GeV}^2$ ($q = 1$). At smallest values of x, the individual *upper curves* always refer to NLO($\overline{\rm MS}$) and the *lower ones* to NNLO($\overline{\rm MS}$)

Table 2. The separate slope $\dot{F}_2^p \equiv \partial F_2^p/\partial \ln Q^2$ and curvature $\ddot{F}_2^p$ contributions to (18) in the $\overline{\rm MS}$ factorization scheme at $x = 10^{-4}$ and for the fixed q-interval in (17) with $\kappa = 0.5\,\mathrm{GeV}^2/(Q^2 + 0.5\,\mathrm{GeV}^2)$. The results are shown for three representative values of Q^2 of this interval. Notice that similarly to (15) we have used $F_2^p(x,Q^2) = A_0(x) + A_1(x)\ln Q^2 + A_2(x)\ln^2 Q^2$, i.e. $\dot{F}_2^p = A_1 + 2A_2 \ln Q^2$ and $\ddot{F}_2^p = 2A_2$

	NLO			NNLO		
Q^2/GeV^2	$\dot{F}_2$	$\kappa\dot{F}_2$	$\ddot{F}_2$	$\dot{F}_2$	$\kappa\dot{F}_2$	$\ddot{F}_2$
1.5	0.3530	0.0883	0.1479	0.3732	0.0933	0.1204
6	0.5580	0.0429	0.1479	0.5401	0.0415	0.1204
12	0.6605	0.0264	0.1479	0.6235	0.0249	0.1204

tive curvature which *increases* as x decreases. Such unique predictions provide a sensitive test of the range of validity of perturbative QCD! This feature is supported by the data shown in Fig. 5a. Future analyses of present precision measurements in this very small-x region (typically $10^{-5} \lesssim x \lesssim 10^{-3}$) should provide additional tests of the theoretical predictions concerning the range of validity of perturbative QCD evolutions.

Finally, the question arises whether the second derivative of F_2^p with respect to the variable q in (15) is indeed dominated by the curvature $\ddot{F}_2^p \equiv \partial^2 F_2^p/\partial(\ln Q^2)^2$ which is directly related to the evolution equations and to experiment, since $\partial_q^2 F_2^p \equiv \partial^2 F_2^p/\partial q^2$ is a linear combination of $\dot{F}_2^p \equiv \partial F_2^p/\partial \ln Q^2 = \mathcal{O}(\alpha_s)$ and $\ddot{F}_2^p = \mathcal{O}(\alpha_s^2)$:

$$\partial_q^2 F_2^p = \left(\frac{Q^2 + 0.5\,\mathrm{GeV}^2}{Q^2}\ln 10\right)^2 \left[-\kappa\dot{F}_2^p + \ddot{F}_2^p\right], \qquad (18)$$

with $\kappa = 0.5\,\mathrm{GeV}^2/(Q^2 + 0.5\,\mathrm{GeV}^2)$. In Fig. 6 we show the two contributions in square brackets separately taking $\kappa = 0.1$ which corresponds to choosing $Q^2 = 4.5\,\mathrm{GeV}^2$, i.e. $q = 1$ as an average of our considered fixed q-interval in (17). The contribution from the slope (first derivative) term $\dot{F}_2^p$ is indeed strongly suppressed and the curvature $\ddot{F}_2^p$ is the dominant contribution in (18) in the small-x region in NLO as well as in NNLO. Since the suppression depends of course on the chosen value for Q^2 in κ we show in Table 2 the separate contributions in square brackets in (18) calculated for three typical values of Q^2 in (17) at a fixed value of $x = 10^{-4}$ in NLO and NNLO. Even at $Q^2 = 1.5\,\mathrm{GeV}^2$ $\ddot{F}_2^p$ dominates over $\kappa\dot{F}_2^p$ and therefore (18) represents a rather clean test of the curvature of a structure function.

4 Conclusions

Perturbative NLO and NNLO QCD evolutions of parton distributions in the (very) small-x region are fully compatible with all recent high-statistics measurements of the Q^2-dependence of $F_2^p(x, Q^2)$ in that region. The results are perturbatively stable and, furthermore, are rather insensitive to the factorization scheme chosen ($\overline{\rm MS}$ or DIS). Therefore additional model assumptions concerning further resummations of subleading small-x logarithms are not required. A characteristic feature of perturbative QCD evolutions is a *positive* curvature $a_2(x)$ which *increases* as x decreases (cf. Fig. 5). This rather unique and perturbatively stable prediction plays a decisive role in probing the range of validity of perturbative QCD evolutions. Although present data are indicative for such a behavior, they are statistically insignificant for $x < 10^{-4}$. Future analyses of present precision measurements in the very small-x region should provide a sensitive test of the range of validity of perturbative QCD and further information concerning the detailed shapes of the gluon and sea distributions as well.

Acknowledgements. This work has been supported in part by the Bundesministerium für Bildung und Forschung, Berlin/Bonn.

References

1. D. Haidt, Eur. Phys. J. C **35**, 519 (2004)
2. M. Glück, C. Pisano, E. Reya, Eur. Phys. J. C **40**, 515 (2005)
3. W.L. van Neerven, A. Vogt, Nucl. Phys. B **568**, 263 (2000)
4. W.L. van Neerven, A. Vogt, Nucl. Phys. B **588**, 345 (2000) [hep-ph/0006154, corrected]
5. J. Blümlein, A. Vogt, Phys. Rev. D **58**, 014020 (1998)
6. W. Furmanski, R. Petronzio, Z. Phys. C **11**, 293 (1982) and references therein
7. S. Moch, J.A.M. Vermaseren, A. Vogt, Nucl. Phys. B **688**, 101 (2004)
8. M. Glück, E. Reya, C. Schuck, Nucl. Phys. B **754**, 178 (2006)
9. A. Vogt, S. Moch, J.A.M. Vermaseren, Nucl. Phys. B **691**, 129 (2004)
10. A. Vogt, Comput. Phys. Commun. **170**, 65 (2005)
11. E. Laenen, S. Riemersma, J. Smith, W.L. van Neerven, Nucl. Phys. B **392**, 162 (1993)
12. S. Riemersma, J. Smith, W.L. van Neerven, Phys. Lett. B **347**, 143 (1995)
13. G. Altarelli, R.K. Ellis, G. Martinelli, Nucl. Phys. B **143**, 521 (1978); B **146**, 544 (1978) [Erratum]
14. G. Altarelli, R.K. Ellis, G. Martinelli, Nucl. Phys. B **157**, 461 (1979)
15. M. Glück, E. Reya, A. Vogt, Z. Phys. C **67**, 433 (1995)
16. H1 Collaboration, C. Adloff et al., Eur. Phys. J. C **21**, 33 (2001)
17. H1 Collaboration, C. Adloff et al., Eur. Phys. J. C **30**, 1 (2003)
18. BCDMS Collaboration, A.C. Benvenuti et al., Phys. Lett. B **223**, 485 (1989)
19. BCDMS Collaboration, A.C. Benvenuti et al., Phys. Lett. B **237**, 599 (1990)
20. NMC Collaboration, M. Arneodo et al., Nucl. Phys. B **483**, 3 (1997)
21. NMC Collaboration, M. Arneodo et al., Nucl. Phys. B **487**, 3 (1997)
22. ZEUS Collaboration, S. Chekanov et al., Eur. Phys. J. C **21**, 443 (2001)
23. S. Forte, G. Altarelli, R.D. Ball, talk presented at DIS 2006, Tsukuba, Japan (April, 2006) [hep-ph/0606323] and references therein
24. A.D. Martin, R.G. Roberts, W.J. Stirling, R.S. Thorne, Eur. Phys. J. C **23**, 73 (2002)
25. J. Pumplin et al., JHEP **7**, 12 (2002) [hep-ph/0201195]